Tuning the frequencies of the normal modes of a nanopillar oscillator through the magnetostatic interaction

D. Mancilla-Almonacid, R. E. Arias, S. Oyarzún, D. Altbir, and S. Allende

Phys. Rev. B **96**, 184424 — Published 21 November 2017

DOI: 10.1103/PhysRevB.96.184424

Tuning the frequencies of the normal modes of a nano-pillar oscillator through the magnetostatic interaction

D. Mancilla-Almonacid,[1] R. E. Arias,[2] S. Oyarzún,[1] D. Altbir,[1] and S. Allende[1]
[1)] *Departamento de Física, CEDENNA, Universidad de Santiago de Chile, USACH, Av. Ecuador 3493, Santiago, Chile*
[2)] *Departamento de Física, CEDENNA, Facultad de Ciencias Físicas y Matemáticas, Universidad de Chile, Av. Blanco Encalada 2008, Santiago, Chile*

A detailed analytical and numerical study of the spin wave modes of the free layer of a nano-pillar spin torque nano-oscillator (STNO) has been performed as a function of the magnetostatic interaction between the free and the fixed magnetic layers. Results for higher frequency normal modes show that the magnetostatic interaction does not appreciably affect the spin wave frequencies and the critical current densities, due to more relevance of the exchange interaction in these modes. For lower frequency normal modes we observe a decrease in frequency and in the critical current density for auto-oscillations when the strength of the magnetostatic interaction between the layers increases, an effect that may be appreciable.

I. INTRODUCTION

During the last decade there has been strong interest in the control of the magnetic behaviour of nanostructures. One of the ways to control the magnetization of a nanomagnet is through the transfer of angular momentum from a spin polarised current by the spin transfer torque (STT) effect[1,2]. Several experiments and theoretical and numerical studies[3–5] have been performed since the experimental confirmation of such effect[6]. The attention has been placed on the potential applications in magnetic data storage technology and spintronics devices where, by using a spin polarised current, it is possible to write information by switching the magnetization in a STT device[7]. Therefore in the last years STT RAM has emerged as an efficient memory technology with a non-volatile character and a reduced power consumption[8]. Nowadays an interesting application of STT devices, i.e. spin torque nano-oscillators (STNO's), occurs in the area of neuro-morphic computing. The STNO's may emulate neuron and synapse networks behaviour through their characteristic nonlinear oscillator dynamics and their coupling[9,10].

Some STT devices such as nano-pillars with metallic spacers, point contacts or magnetic tunnel junctions are composed of two ferromagnetic layers separated by a non-magnetic spacer. The first ferromagnetic layer is magnetically fixed while the magnetization of the second ferromagnetic layer is free to move in response to an external stimulus. When a current is injected into the system, electrons pass through the fixed layer and become spin-polarised. Then this spin polarised current reaches the second ferromagnetic layer whose dynamic magnetization in general is not collinear with the first, and thus some current angular momentum is transferred to the free layer. If the current density is large enough, a stable precession of the magnetization of the free layer may be reached in the microwave range[11]. In most works the non-magnetic spacer is considered sufficiently wide to neglect both the magnetostatic and the Ruderman-Kittel-Kasuya-Yosida (RKKY) interactions between the two ferromagnetic layers. Besides, only few papers address the influence of the fixed layer thickness. For example, S. Urazhdin et al.[12] made experimental measurements of the dynamics induced by a polarised current across a thin spin valve device. They considered that the dimensions of the free layer are fixed and the thickness of the reference layer is comparable or smaller than the free layer thickness. For the fixed layer thickness the authors considered 2, 5, and 8 nm. The coupling between both ferromagnetic layers results in a reduction of the precession onset current. Also Z. Hou et al.[13] studied the stability of the reference layer given by a mutual STT effect considering the macro-spin approximation for both ferromagnetic layers. They concluded that the consideration of that effect is important to understand the spin-torque switching. We also mention a recent experimental-theoretical study[14] on the influence of inter-layer coupling on the spin torque driven excitations of a spin torque oscillator.

As already mentioned, nano-pillars have a non-magnetic spacer between the ferromagnetic layers. The thickness of this spacer is generally from 1 nm to 100 nm[15–24]. The spacer thickness must be smaller than the spin diffusion length, usually a hundred of nanometers, to keep the spin polarization of the current[25]. However, from another side, the spacer should be thick enough to avoid RKKY interaction between the ferromagnetic layers of the nano-pillar. In this case, magnetostatic interaction between the free and the fixed layers can play an appreciable role. There are several experimental systems in which both conditions are satisfied[18–24]. Therefore, in this work we focused on the effect of the magnetostatic interaction between the ferromagnetic layers of a nano-pillar with a circular cross section using a standard Hamiltonian formalism. We studied the normal modes of the free layer as a function of the fixed layer thickness neglecting the RKKY interaction. Specifically, we have studied the normal modes, its frequency dependence, shape and critical current to induce stable or auto-oscillations. We also studied the normal modes dependency on non-magnetic spacer thickness and magnetic material of the fixed layer. We found that for lower

frequency normal modes, the frequency and critical current density decrease when the fixed layer thickness increases or the non-magnetic spacer thickness decreases. In this scenario, the shape of the lower normal modes is not affected by the magnetostatic interaction between the layers. On the other hand for higher normal modes, the frequency and the critical current density are not affected by the magnetostatic interaction between the layers. Thus STT nano-pillar oscillators can be controlled in terms of frequency range or current density by material engineering, and geometry design.

This paper is organized as follows: in Section II we describe the model and formalism used to determine the equilibrium magnetization, the spin wave modes and the critical current densities, in Section III we present and discuss our results, and finally in Section IV conclusions are presented.

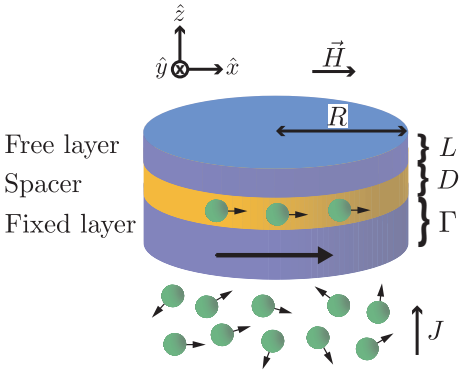

FIG. 1. Geometry and parameters of the cylindrical nano-oscillator considered. A current is injected into the structure, its spin direction is polarised as it passes through the fixed layer.

II. MODEL

We consider a nano-pillar device composed of two ferromagnetic layers separated by a non-magnetic metallic spacer with a circular cross section of radius R, as shown in Fig. 1. The bottom layer has its magnetization fixed while the magnetization of the top layer is free. The free (fixed) layer has a thickness L (Γ) and a saturation magnetization M_s ($M_{\rm fix}$). The non-magnetic metallic spacer has a thickness D, smaller than the spin diffusion length (l_{sf}), and large enough to neglect the RKKY interaction between the two ferromagnetic layers. For example, if the spacer is copper, the spin diffusion length is l_{sf} =350 nm at $T = 293$ K[25]. When we study the effect of D on the normal modes of the free layer, we choose the minimum D equal to 2 or 3 nm depending on the material magnetization of the fixed layer. On the other hand, when we study the normal modes with constant spacer thickness, we consider $D = 5$ nm. The latter value was chosen to be sure that RKKY interaction does not affect our calculations[26].

To find the normal modes of the free layer as a function of the magnetostatic interaction between the ferromagnetic layers, we analyse the magnetization dynamics through the Landau-Lifshitz-Slonczewski equation (LLS)[27] and the Hamiltonian formalism[28] to solve it. This section is organised into three subsections: a brief explanation of the LLS equation, the Hamiltonian formalism, and a final subsection that describes how the equilibrium magnetization, spin wave normal modes and critical current densities are obtained.

A. Magnetization dynamics of the free layer

The magnetization dynamics of the free layer induced by a spin polarised current is described by the Landau-Lifshitz-Slonczewski equation

$$\frac{d\vec{m}}{d\tau} = -\vec{m}\times\vec{h}_{\rm eff} - \alpha\vec{m}\times(\vec{m}\times\vec{h}_{\rm eff}) + \beta J\vec{m}\times(\vec{m}\times\hat{p}) \ , \tag{1}$$

where $\vec{m} = \vec{M}/M_s$ is the normalised magnetization vector of the free layer. α is the damping parameter, and the time is normalized by $\tau = |\gamma|4\pi M_s t$, with $|\gamma| = 1.76\cdot 10^7 {\rm Oe}^{-1}\cdot {\rm s}^{-1}$ being the gyromagnetic ratio[29]. J is the applied current density and $\hat{p}$ is the spin polarization direction. The coefficient β is defined as follows[1]:

$$\beta = \frac{h}{(4\pi M_s)^2 eL}\left[-4 + (3+\cos\theta)\frac{(1+P)^3}{4P^{3/2}}\right]^{-1} , \tag{2}$$

where h is the Planck constant, e the electron charge, P the polarization and θ the angle between the magnetization and the spin polarization direction. $\vec{h}_{\rm eff}$ is the normalized effective field, where it is equal to $\vec{h}_{\rm eff} = \vec{H}_{\rm eff}/4\pi M_s = -\delta\mathcal{U}_{\rm eff}/\delta\vec{m}$, where $\mathcal{U}_{\rm eff} = \mathcal{U}_Z + \mathcal{U}_D + \mathcal{U}_E + \mathcal{U}_I$ is the normalized free layer magnetic energy. In the $\mathcal{U}_{\rm eff}$ expression, $\mathcal{U}_Z$ is the energy associated with the external applied field; $\mathcal{U}_D$ the demagnetizing free layer energy averaged over the layer thickness ; $\mathcal{U}_E$ the exchange interaction energy; and $\mathcal{U}_I$ the energy related to the magnetostatic interaction between the two ferromagnetic layers. The magnetic anisotropy energy for the free layer was neglected because we consider a soft magnetic material, Permalloy. The last term in Eq. (1) is the normalised spin transfer torque term. We neglected the out plane spin transfer torque due to the non-magnetic spacer is a metal[30].

B. Hamiltonian formalism

The LLS equation conserves the magnitude of the magnetization ($|\vec{m}^2| = 1$). Then, the three components of

the magnetization are not independent of each other, and only two of them to are necessary to describe the dynamics. For this reason and because the normalised equilibrium magnetization is almost saturated $\vec{m}^{eq} \approx m_x\hat{x}$, it is convenient to introduce the complex variable $a(\vec{\rho},\tau)$ through the classical Holstein-Primakoff transformation, as used by Mancilla-Almonacid and Arias in Ref. 31. That is,

$$\left.\begin{array}{c} m_x = 1 - aa^* \\ m_y = ((a-a^*)/2i)\sqrt{2-aa^*} \\ m_z = ((a+a^*)/2)\sqrt{2-aa^*} \end{array}\right\} \quad \Leftrightarrow \quad a = \frac{im_y + m_z}{\sqrt{1+m_x}} \,, \tag{3}$$

where a and a^* are small perturbations of the equilibrium saturated state. They correspond to the classical analogue of the magnon creation and annihilation operators. Using this transformation, Eq. (1) is transformed into the following equation for a:

$$i\frac{da}{d\tau} \approx (1-i\alpha)\frac{\delta \mathcal{U}_{\text{eff}}}{\delta a^*} + i\beta J a \,, \tag{4}$$

where the non-linear terms of the dissipation and spin transfer torque have been neglected, as we are interested in the linear dynamics. The expressions for the energies as a function of a and a^* are found in Appendix A (see equation A3 for $\mathcal{U}_Z(a,a^*)$, equation A5 for $\mathcal{U}_E(a,a^*)$, equation A11 for $\mathcal{U}_D(a,a^*)$ and equation A16 for $\mathcal{U}_I(a,a^*)$). To describe the free layer dynamics by appropriate variables, we introduce a change of variables from $a(\vec{\rho},\tau)$ to $a_{mj}(\tau)$, which are the coefficients of an expansion in Bessel functions as follows

$$a(\vec{\rho},\tau) = N_{00}a_{00}(\tau) + \sum_{\substack{m=-\infty \\ j=1}}^{\infty} N_{mj}a_{mj}(\tau)J_m\left(\frac{\chi_{mj}\rho}{R}\right)e^{im\phi} \,, \tag{5}$$

where ρ and ϕ are the radial and polar coordinates, and J_m are the Bessel functions of the first kind of order m. Since we consider free boundary conditions at the edges of the free layer, that is $\partial\vec{m}/\partial\rho\big|_{\rho=R} = 0$, thus the constants χ_{mj} must satisfy $J'_m(\chi_{mj}) = 0$, i.e. they are the zeroes of J'_m. In writing Eq. (5) we have considered that the free layer is very thin, that is $L \sim l_E$, where l_E is the exchange length of the free layer material. Then, its magnetization does not depend on z and thus we can average the fields and energies over this variable. Finally, the magnetization dynamics in the variables $\{a_{mj}, a^*_{mj}\}$ reads (the transformation $\{a, a^*\} \to \{a_{mj}, a^*_{mj}\}$ is canonical for the conservative equations, i.e. it maintains the Hamiltonian form of those equations):

$$i\frac{da_{mj}}{d\tau} \approx (1-i\alpha)\frac{1}{V}\frac{\partial \mathcal{U}_{\text{eff}}}{\partial a^*_{mj}} + i\beta J a_{mj} \,, \tag{6}$$

with $V = \pi R^2 L$ the free layer volume. The coefficients $N_{00} = 1$ and $N_{mj} = 1/\sqrt{-J_m(\chi_{mj})J''_m(\chi_{mj})}$ are normalization constants with $\partial a/\partial a_{mj} = V\delta a^*_{mj}/\delta a^*$. Expressions for the energies as a function of the variables a_{mj} and a^*_{mj} are found in Appendix B.

C. Equilibrium magnetization, spin waves and critical current density

Before studying the dynamics of the system, we obtained the equilibrium magnetization state for the free layer. Therefore, we solved

$$\left.\frac{\partial \mathcal{U}_{\text{eff}}}{\partial a^*_{mj}}\right|_{eq} = 0 \,. \tag{7}$$

This equation represents a system of non-linear equations that can be solved numerically by using an extension of the Newton-Raphson method[32]. The solutions of these equations are the values of a^{eq}_{mj}, that represent the equilibrium configuration of the free layer magnetization.

To study the magnetization dynamics we write $a_{mj} = a^{eq}_{mj} + \tilde{a}_{mj}$, where $\tilde{a}_{mj}$ represent small perturbations around the equilibrium values a^{eq}_{mj}. Then, at linear order Eq. (6) can be approximated by using an expansion in Taylor series around the equilibrium state, i.e.

$$\begin{aligned} i\frac{d}{d\tau}\begin{pmatrix} \tilde{a}_{mj} \\ \tilde{a}^*_{mj} \end{pmatrix} &= \begin{pmatrix} A^{m'j'}_{mj} & B^{m'j'}_{mj} \\ -B^{m'j'*}_{mj} & -A^{m'j'*}_{mj} \end{pmatrix}\begin{pmatrix} \tilde{a}_{m'j'} \\ \tilde{a}^*_{m'j'} \end{pmatrix} \\ &= \mathbf{M}\begin{pmatrix} \tilde{a}_{m'j'} \\ \tilde{a}^*_{m'j'} \end{pmatrix} \,, \end{aligned} \tag{8}$$

where $A^{m'j'}_{mj}$ and $B^{m'j'}_{mj}$ are

$$A^{m'j'}_{mj} = (1-i\alpha)\left.\frac{\partial^2 \mathcal{U}_{\text{eff}}}{\partial a^*_{mj}\partial a_{m'j'}}\right|_{eq} + i\beta J\delta^m_{m'}\delta^j_{j'} \,, \tag{9a}$$

$$B^{m'j'}_{mj} = (1-i\alpha)\left.\frac{\partial^2 \mathcal{U}_{\text{eff}}}{\partial a^*_{mj}\partial a^*_{m'j'}}\right|_{eq} \,. \tag{9b}$$

In the previous equations, $\mathbf{M}$ is a diagonalizable matrix that can be decomposed as $\mathbf{M} = \mathbf{PDP}^{-1}$, where $\mathbf{D}$ is a diagonal matrix constructed from the corresponding eigenvalues of $\mathbf{M}$, and $\mathbf{P}$ is an invertible matrix composed of the eigenvectors of $\mathbf{M}$. Since the variables $\tilde{a}_{mj}$ do not represent the normal modes of oscillation, we performed a Bogoliubov transformation to obtain the normal modes:

$$\begin{pmatrix} \tilde{a}_{mj} \\ \tilde{a}^*_{mj} \end{pmatrix} = \begin{pmatrix} \lambda^n_{mj} & -\mu^n_{mj} \\ -\mu^{n\,*}_{mj} & \lambda^{n\,*}_{mj} \end{pmatrix}\begin{pmatrix} b_n \\ b^*_n \end{pmatrix} = \mathbf{P}\begin{pmatrix} b_n \\ b^*_n \end{pmatrix} \,. \tag{10}$$

Replacing this transformation in Eq. (8), one obtains the following linear diagonal equations for the dynamics of the amplitudes b_n and b^*_n of mode n, given by

$$\begin{aligned} i\frac{d}{d\tau}\begin{pmatrix} b_n \\ b^*_n \end{pmatrix} &= \begin{pmatrix} \omega_n + i\gamma_n & 0 \\ 0 & -\omega_n + i\gamma_n \end{pmatrix}\begin{pmatrix} b_n \\ b^*_n \end{pmatrix} \\ &= \mathbf{D}\begin{pmatrix} b_n \\ b^*_n \end{pmatrix} \,, \end{aligned} \tag{11}$$

where ω_n and γ_n are real variables. The solutions of Eq. (11) are $b_n(\tau) = b^0_n e^{(-i\omega_n+\gamma_n)\tau}$, with the dimensionless quantity ω_n the angular frequency of oscillation of

mode n. Then, the oscillation frequency of this mode is $f_n^N = 2M_s|\gamma|\omega_n$, where the super-index N represents that the frequencies are obtained by numerical calculations. The linear decay coefficient of mode n is γ_n, and it depends on the applied current density, $\gamma_n(J)$. The critical current density, i.e. the minimum current density to induce self oscillations on the free layer magnetization for a normal mode, can be obtained by equating $\gamma_n(J_{c,n}^N) = 0$, where the super-index N represents that the critical current is obtained by numerical calculations. Then, if $\gamma_n(J) > 0$ it is possible to excite self oscillations of the normal modes, while if $\gamma_n(J) < 0$ these are not induced. It is important to mention that for for $\gamma_n(J) > 0$, there is not necessarily only one mode that is auto-oscillating, that is, several normal modes can coexist. Moreover, this condition can generate an incoherent dynamic or even the magnetization can be reversed depending on the current magnitude. In our case, we will study only the current that satisfies $\gamma_n(J) = 0$ for a certain n mode, that is, the critical current $J_{c,n}^N$ obtained gives us the current where the n mode begins to auto-oscillate.

III. RESULTS AND DISCUSSIONS

The system we have considered consists of a free layer of permalloy, a copper spacer and a fixed layer of permalloy or cobalt. For our calculations we considered as fixed the geometrical parameters $R = 50$ nm and $L = 5$ nm. For permalloy we have used: $M_s = 800$ emu/cm^3, exchange stiffness constant $A = 1.3 \cdot 10^{-6}$ erg/cm, and an exchange length $l_E = 5.7$ nm. With respect to the calculation of the magnetostatic interaction between the magnetic layers, we have used two materials for the fixed layer: cobalt with $M_{\text{fix}} = 1400$ emu/cm^3 and permalloy with $M_{\text{fix}} = 800$ emu/cm^3, see Refs. 19–24, 33, and 34. The thickness of the fixed layer was variated from 0 to 10 nm for cobalt and from 0 to 20 nm for permalloy. For values bigger than $\Gamma = 10$ nm for cobalt and $\Gamma = 20$ nm for permalloy, the magnetostatic interaction field becomes greater than the external applied field. Both fields are opposed to each other, so the parallel state is no longer stable and the free layer could revert its magnetization generating an anti-parallel state. In the same way, the change of variable $m_x = 1 - aa^*$ is not valid anymore. In order to saturate the magnetization of the fixed layer with a large thickness, an external field can be applied or also this layer can be placed in contact with an antiferromagnetic layer. To solve the LLS equation and to describe the magnetization dynamics of the free layer, we have used the following parameters: $\alpha = 0.01$, the spin polarization of permalloy $P = 0.3$ (see Ref. 35), $\theta = 0$, and the spin polarization direction is chosen as $\hat{p} = \hat{x}$. In all the cases we used an applied external field $H_x = 1$ kOe. The limits of the summation in Eq. (5) are given from $m = -4$ to $m = 4$ and from $j = 1$ to $j = 4$.

In the following three subsections contain our results and discussions. In the first subsection we focus on the equilibrium magnetization configuration of the free layer as a function of the fixed magnetic layer. In the second part, we discuss how the shape and frequency of the normal modes change when we consider a fixed magnetic layer with different parameters. Finally, we study the variation of the critical current density when taking into account changes of the fixed magnetic layer.

A. Equilibrium magnetization

In this subsection we will show how the equilibrium magnetization of the free layer is modified when the magnetostatic interaction with the fixed layer is taken into account. This equilibrium magnetization is obtained from Eq. (3) as a function of the complex variable $a(\vec{\rho}, \tau)$ defined in Eq. (5). The variable $a(\vec{\rho}, \tau)$, in the equilibrium configuration, is obtained by solving Eq. (7). Our results for the equilibrium magnetization of the free layer in the absence of an applied current are illustrated in Fig. 2. The vectors represent the in-plane magnetization, i.e., the normalized magnetization components m_x and m_y, while the out-plane normalized magnetization, m_z, is represented by a color scale. Fig. 2(a) illustrates the case where the system does not interact with a fixed layer, thus the equilibrium magnetization in the free layer is completely in-plane with $m_z = 0$. Fig. 2(b) illustrates results for an interacting system defined by a fixed permalloy layer with $\Gamma = 20$ nm and a spacer of $D = 5$ nm. The interaction field in the free layer is in opposite direction to the external applied field. To consider the change of variables of Eq. (3) properly, the absolute interaction field must be smaller than the absolute applied field. In figure 2(b), the absolute normalized average interaction field corresponds approximately to 0.08, which is less than the absolute normalized applied field (0.1). From this figure, we observe that there are regions where the value of the m_z is different to zero, then the equilibrium state of the magnetization is different from the case without the fixed layer.

B. Frequencies and shapes of the normal modes

In this section we discuss how the frequencies of the normal modes are modified by the magnetostatic interaction between the layers. These frequencies, f_n^N, are calculated following the procedure explained before Eq. (10), i.e. it involves the diagonalization of matrix M of Eq. (8) for the dynamic perturbations around the equilibrium configuration. The Fig. 3 illustrates the first three frequencies of the normal modes as a function of the fixed layer thickness. In this figure we observe that the frequency of each mode decreases when the fixed layer thickness increases.

We also studied the dependency of the frequency of each mode on the non-magnetic spacer thickness. From

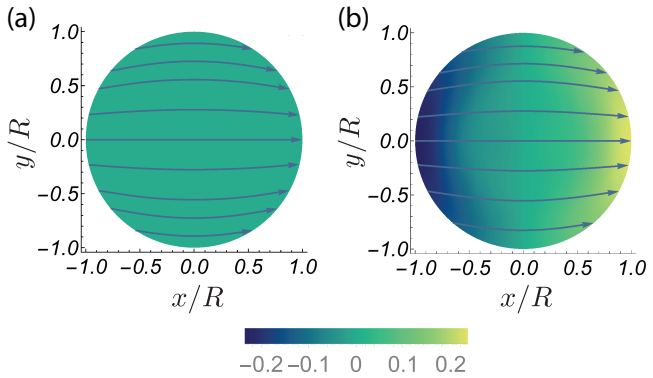

FIG. 2. Equilibrium magnetization of the free layer. (a) The magnetostatic interaction between the free and the fixed layers is neglected. (b) The magnetostatic interaction between the free and the fixed layers is considered. The vectors are associated with the in-plane components of the magnetization, m_x and m_y, and the color is associated with the out-plane component of the magnetization, m_z.

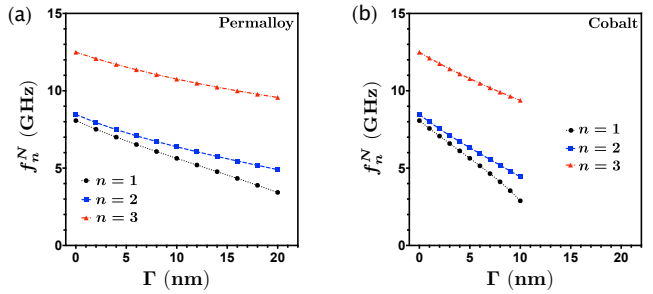

FIG. 3. Frequencies of the first three modes as a function of the fixed layer thickness. (a) The free and fixed layers are made of permalloy. (b) The free layer is made of permalloy and the fixed layer is made of cobalt. The thickness of the metallic spacer is $D = 5$ nm.

Fig. 4, we observe that the frequency decreases when the spacer thickness diminishes, due to the concomitant increase of the magnetostatic interaction between the layers. Additionally, it is possible to see that the nature of the magnetic material also affects the frequency changes of the normal modes. This effect is evidenced in Figs. 3 and 4 where, for the harder magnetic material, the change in frequencies is more significant. In Fig. 4, the smaller thickness for the non-magnetic spacer is 2 nm for permalloy and 3 nm for cobalt. This, since the different saturation magnetizations of cobalt and permalloy require different thicknesses of the spacers to prevent that the demagnetizing field generated by the fixed layers could reverse the magnetization in the free layer. We could access to smaller thicknesses if we increase the external field, as explained in Appendix C.

In order to better understand these results, we did a theoretical analysis considering two approximations.

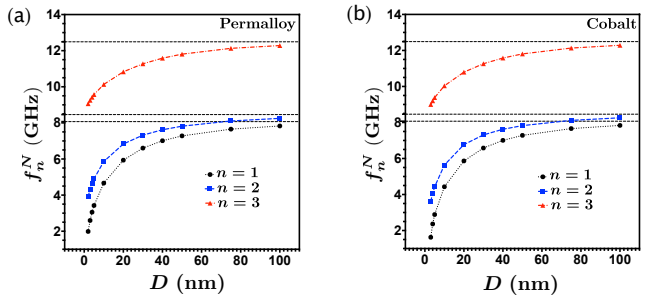

FIG. 4. Frequencies of the first three modes as a function of the non-magnetic spacer thickness. (a) The free and fixed layers are made of permalloy and the thickness of the fixed layer is $\Gamma = 20$ nm. (b) The free layer is made of permalloy and the fixed layer is made of cobalt with a thickness equal to $\Gamma = 10$ nm. The horizontal dashed lines represent the frequencies of the normal modes without the effect of the fixed layer.

The first one assumes that the demagnetizing field of the free layer can be approximated by $\vec{H}_D = -4\pi M_z \hat{z}$, an approach frequently known as the thin film limit ($L \ll R$)[36]. In the absence of magnetostatic interaction between the free and the fixed layers, the free layer eigenfrequencies are

$$f^A_{mj}(\Gamma = 0) = 2M_s|\gamma|\sqrt{(h_x + h_E^{mj})(h_x + h_E^{mj} + 1)}\,, \tag{12}$$

see Ref. 31. In this equation, the super-index A represents that the frequencies are obtained by analytical calculations, $h_x = H_x/(4\pi M_s)$ is the normalised external applied field, $h_E^{mj} = (\chi_{mj} l_E/R)^2$ is the normalised exchange field, and l_E is the exchange length (see A 2). The second approach averages the normalised magnetostatic field induced by the fixed layer over the free layer volume. In this case only the x component of this normalised average field is different to zero, $\langle h_I^x \rangle_V$, and it is given by

$$\langle h_I^x \rangle_V = -\frac{M_{\rm fix}}{M_s}\int_0^\infty \frac{J_1^2(q)(1-e^{-\frac{q\Gamma}{R}})(1-e^{-\frac{qL}{R}})e^{-\frac{qD}{R}}}{2q^2\frac{L}{R}}dq\,, \tag{13}$$

where the sub-index indicates the average over the volume of the free layer. Our analytical model includes these two approximations, and therefore the frequencies of the normal modes in the analytical model can be rewritten as follows:

$$\begin{aligned} f^A_{mj} &= 2M_s|\gamma|\sqrt{(h_x + h_E^{mj} + \langle h_I^x \rangle_V)(1 + h_x + h_E^{mj} + \langle h_I^x \rangle_V)} \\ &= f^A_{mj}(\Gamma = 0)\sqrt{\left(1 + \frac{\langle h_I^x \rangle_V}{h_x + h_E^{mj}}\right)\left(1 + \frac{\langle h_I^x \rangle_V}{1 + h_x + h_E^{mj}}\right)}. \end{aligned} \tag{14}$$

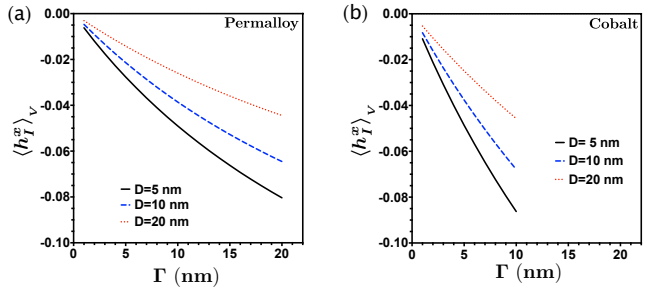

FIG. 5. Normalised average magnetostatic field as a function of the fixed layer thickness for $D = 5$ nm, 10 nm and 20 nm. (a) The free and fixed layers are made of permalloy. (b) The free layer is made of permalloy and the fixed layer is made of cobalt.

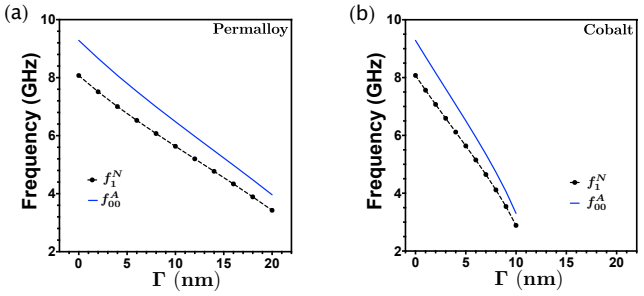

FIG. 6. Frequency of the uniform mode as a function of the fixed layer thickness $D = 5$ nm. (a) The free and fixed layers are made of permalloy. (b) The free layer is made of permalloy and the fixed layer is made of cobalt. The blue line corresponds to the analytic formula obtained by the analytical model, see Eq. (14). The black dots correspond to the numerical solution previously found from Eq. (11) for $n = 1$ (see figure 3(a) for permalloy and figure 3(b) for cobalt).

Fig. 5 illustrates the normalised average magnetostatic field $\langle h_I^x \rangle_V$ as a function of the fixed layer thickness. We considered in the calculation different values for the spacer thickness and magnetic materials, as shown in Figs. 5(a) for permalloy and 5(b) for cobalt. First, we observe that the strength of $\langle h_I^x \rangle_V$ depends on the magnetic material of the fixed layer and the spacer thickness. With the same geometrical parameters the fixed layer of cobalt produces a stronger field than permalloy. This is the reason why we only plot up to $\Gamma = 10$ nm as displayed in figure 3(b), since for values greater than $\Gamma = 10$ nm, the normalised average magnetostatic field can be greater than the normalised external applied field, and Eq. (3) will not be valid. In addition, we observe that the normalised average magnetostatic field is negative and goes to zero when the fixed layer thickness decreases. In this way one may understand why the frequencies obtained in Fig. 3 decrease when the thickness of the fixed layer increases or the non-magnetic spacer thickness decreases. These results are confirmed in Fig. 6 where the oscillation frequency of the uniform mode or macro-spin mode in the analytical model, f_{00}^A, and the frequency mode previously obtained numerically for the mode $n = 1$ also called quasi-uniform, f_1^N are depicted (see Fig. 3(a) for permalloy and Fig. 3(b) for cobalt). Although differences in oscillation frequencies are observed, the decay is similar. The analytical model exhibits the same behaviour than our numerical results, and a better agreement for large values of Γ. The frequency differences between the analytical and numerical models are due to the thin film limit approximation of the demagnetizing field that we use in our analytical model. A better agreement between theory and numerical analysis is obtained when Γ increases, because the magnetostatic interaction field increases correspondingly, making, in the comparison, the demagnetizing field less relevant.

From Eq. (14), we observe that the effect of the fixed layer on the free layer is limited for higher normal modes. If $|\langle h_I^x \rangle_V| \ll |h_x + h_E^{mj}|$, then $f_{mj}^A \approx f_{mj}^A(\Gamma = 0)$. Therefore, the fixed layer does not affect the higher normal mode frequencies. In the analytical model we calculated the condition for wich the frequencies are not affected by any fixed layer thickness and any non-magnetic spacer thickness when $|h_x| > |\langle h_I^x \rangle_V|$. Then, we have $f_{mj}^A \approx f_{mj}^A(\Gamma = 0)$ if

$$\chi_{mj} \gg \frac{R}{l_E}\sqrt{\frac{H_x}{4\pi M_s}}. \tag{15}$$

Replacing the parameters used in our calculations in Eq. (15), we have the next condition $\chi_{mj} \gg 2.77$. To understand Eq. (15), we need to observe Fig. 7. This figure illustrates the numerical and analytical frequency variations as a function of the normal modes, where the numerical frequency variation is defined by

$$\Delta f_n^N(\Gamma, D) = 100 \times (f_n^N(\Gamma = 0) - f_n^N)/f_n^N(\Gamma = 0)\ , \tag{16}$$

with $f_n^N(\Gamma = 0)$ as the frequency mode calculated numerically with a non-fixed layer, and the analytical frequency variation is defined by using the analytical model, i.e.,

$$\Delta f_{mj}^A(\Gamma, D) = 100 \times (f_{mj}^A(\Gamma = 0) - f_{mj}^A)/f_{mj}^A(\Gamma = 0)\ . \tag{17}$$

For $\Delta f_n^N(\Gamma, D)$ and $\Delta f_{mj}^A(\Gamma, D)$, we have chosen $\Gamma = 20$ nm and $D = 5$ nm for permalloy and $\Gamma = 10$ nm and $D = 5$ nm for cobalt. These geometrical parameters give the biggest drop in frequency in our calculations. In the analytical model, each χ_{mj} represents two normal modes if $m \neq 0$ (there is degeneracy), and one normal mode if $m = 0$. The lower values of χ_{mj} correspond to the lower normal modes. In our case, we count the first ten normal modes denoted in Table I.

From Fig. 7, we observe that the frequency variation starts approximately in 60% for the first mode and decreases when we increase the normal mode number n.

n	m	j	χ_{mj}
1	0	0	0
2, 3	1	1	1.84
4, 5	2	1	3.05
6	0	1	3.83
7, 8	3	1	4.20
9, 10	4	1	5.31

TABLE I. The table shows the values of χ_{mj} necessary to calculate $\Delta f^A_{mj}(\Gamma, D)$ for the lower normal modes. n corresponds the normal mode.

The increment of the normal mode number, in the analytical model, means an increment of the value of χ_{mj}. Therefore, if we take an n that has a $\chi_{mj} \gg 2.77$, then the frequency variation goes to zero, i.e. the higher normal modes are not affected by the magnetostatic interaction between the layers.

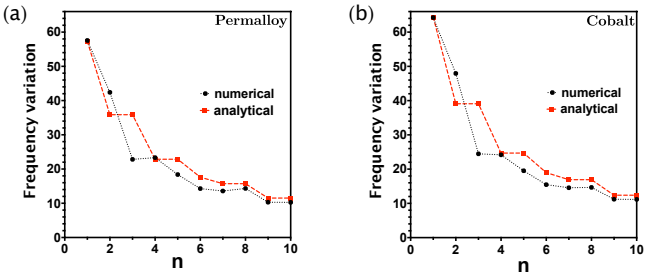

FIG. 7. Frequency variation from Eqns. (16) and (17) as a function of the normal modes. (a) The free and fixed layers are made of permalloy with $\Gamma = 20$ nm and $D = 5$ nm. (b) The free layer is made of permalloy and the fixed layer is made of cobalt with $\Gamma = 10$ nm and $D = 5$ nm. The dot black line corresponds to $\Delta f^N_n(\Gamma, D)$. The dashed blue line corresponds to $\Delta f^A_{mj}(\Gamma, D)$.

In the second part of this subsection, we discuss the magnetostatic interaction effect on the shape of the normal modes. In absence of dissipation and spin transfer torque effect, the magnetization dynamics of the component m_z is plotted in Fig. 8, which at linear order is

$$m_z = \frac{\tilde{a} + \tilde{a}^*}{\sqrt{2}} = \frac{1}{\sqrt{2}} \sum_n \sum_{mj} b^0_n N_{mj} J_m(\chi_{mj}\rho/R) \times [(\lambda^n_{mj} e^{-i\omega_n \tau} - \mu^n_{mj} e^{i\omega_n \tau}) e^{im\phi} + c.c] \,. \quad (18)$$

In this figure, the fixed layer is made of permalloy and has a thickness of $\Gamma = 20$ nm and a non-magnetic spacer thickness equal to $D = 5$ nm. With these geometrical parameters, the magnetostatic interaction between the permalloy layers is the strongest in our calculations, see Fig. 5. The shape of the first three normal modes are compared in the absence (Fig. 8(a), Fig. 8(c) and Fig. 8(e)) and in presence (Fig. 8(b), Fig. 8(d) and Fig. 8(f)) of the magnetostatic interaction between the free and the fixed layers. We observe that they are essentially very similar. Therefore, it is possible to change the oscillation frequencies as a function of the fixed layer thickness without changing the shape of the normal modes.

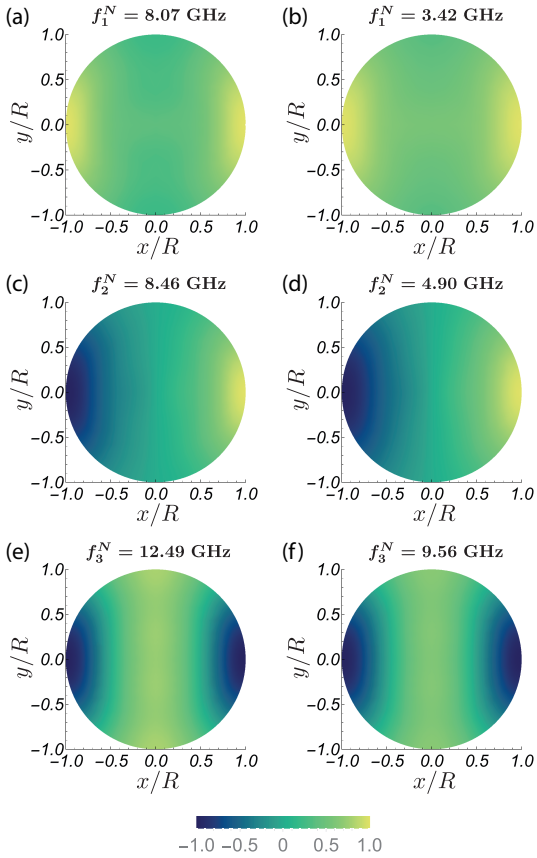

FIG. 8. Shape of the normal modes associated with the magnetization dynamics of the component m_z for the first normal mode (first row), the second normal mode (second row), and the third normal mode (third row). This figure shows different systems at $\tau = 0$. The left column does not consider the magnetostatic interaction between the free and the fixed layers in the calculations. The right column considers the magnetostatic interaction between the ferromagnetic layers. The frequencies were set to show that there is a frequency change, but no modification in the shape of the normal modes were observed In this case, both magnetic layers are made of permalloy. We assumed that m_z is in the range between $[-1, 1]$ (this is arbitrary since these are linear modes).

C. Critical current density

When a current runs through the nano-pillar, it is possible to induce oscillations on the free layer magnetization if the current exceeds a certain threshold, called the critical current density $J^N_{C,n}$. Fig. 9 illustrates the lowest critical current density for $n = 1$, $J^N_{C,1}$, as a function of the fixed layer thickness for $D = 5$ nm and $D = 20$

nm. In the same way as the oscillation frequencies are modified, the critical current density is modified if the magnetostatic interaction is considered, i.e., the critical current density decreases if the fixed layer thickness increases or the non-magnetic spacer decreases. In addition, while the harder it is the fixed layer material, the greater it is the critical current density variation. To

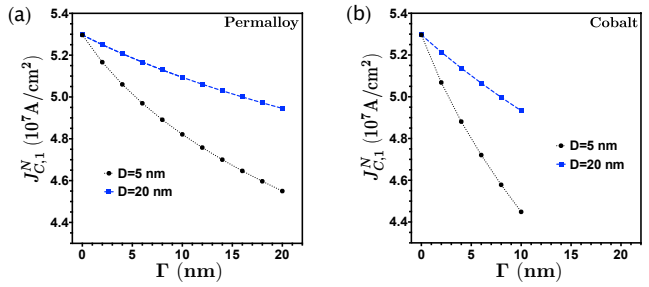

FIG. 9. Critical current density necessary to induce self-oscillations in the lowest normal mode as a function of the fixed layer thickness, at $D = 5$ nm (dots) and $D = 20$ nm (squares). (a) The free and fixed layers are made of permalloy. (b) The free layer is made of permalloy and the fixed layer is made of cobalt.

understand the results plotted in Fig. 9 and obtain an analytical expression, we have used the analytical model. The critical current density without the magnetostatic interaction between the layers, in the analytical model is

$$J^A_{C,mj}(\Gamma = 0) = \alpha(h_x + h_E^{mj} + 1/2)/\beta \,, \qquad (19)$$

where the super-index A represents that the critical current is obtained by analytical calculations. If we consider the magnetostatic interaction, where the normalized average magnetostatic field from the fixed layer is $\langle h_I^x \rangle_V$ (see Eq. (13)), the critical current density in the analytical model can be rewritten as:

$$\begin{aligned} J^A_{C,mj} &= \frac{\alpha}{\beta}\left(\frac{1}{2} + h_x + h_E^{mj} + \langle h_I^x \rangle_V\right) \\ &= J^A_{C,mj}(\Gamma = 0)\left(1 + \frac{\langle h_I^x \rangle_V}{\frac{1}{2} + h_x + h_E^{mj}}\right) \,, \end{aligned} \qquad (20)$$

where $h_x = H_x/(4\pi M_s)$ and $h_E^{mj} = (\chi_{mj} l_E/R)^2$. Eq. (20) explains the decrease observed in Fig. 9. It is because $\langle h_I^x \rangle_V$ is negative. This could be experimentally useful due to the possibility to decrease the critical current density about 20% in both materials (permalloy and cobalt). If $|\langle h_I^x \rangle_V| \ll |1/2 + h_x + h_E^{mj}|$, then $J^A_{C,mj} \approx J^A_{C,mj}(\Gamma = 0)$, therefore the fixed layer does not affect the critical current densities at higher normal modes. In the analytical model, we can calculate the condition where the critical current densities are not affected by any fixed layer thickness and any non-magnetic spacer thickness when $|h_x| > |\langle h_I^x \rangle_V|$. Then, we have $J^A_{C,mj} \approx J^A_{C,mj}(\Gamma = 0)$ if $1/2 + h_E^{mj} \gg |h_x|$ or:

$$\frac{R^2}{2l_E^2} + \chi_{mj}^2 \gg \frac{|H_x|R^2}{4\pi M_s l_E^2}. \qquad (21)$$

In our calculation we get from Eq. (21) the next condition $38.47 + \chi_{mj}^2 \gg 7.69$. If we compare the expressions for the conditions of Eqns. (15) and (21), we observe that the critical current density has less variation than the frequency for the same normal mode, and the current density variation decreases faster than the frequency variation. Fig. 10 confirms the predictions of the conditions of Eqns. (15) and (21). This figure shows the numerical and analytical critical current density variation as a function of the normal modes, where the numerical critical current density variation (percentage) is defined by

$$\Delta J^N_{C,n}(\Gamma, D) = 100 \times (J^N_{C,n}(\Gamma = 0) - J^N_{C,n})/J^N_{C,n}(\Gamma = 0) \,, \qquad (22)$$

with $J^N_{C,n}(\Gamma = 0)$ as the critical current density calculated numerically with a non-fixed layer, and the analytical critical current density variation (percentage) is defined by using the analytical model, i.e.,

$$\begin{aligned} &\Delta J^A_{C,mj}(\Gamma, D) \\ &\quad = 100 \times (J^A_{C,mj}(\Gamma = 0) - J^A_{C,mj})/J^A_{C,mj}(\Gamma = 0) \,. \end{aligned} \qquad (23)$$

For $\Delta J^N_{C,n}(\Gamma, D)$ and $\Delta J^A_{C,mj}(\Gamma, D)$, we have chosen $\Gamma = 20$ nm and $D = 5$ nm for permalloy, and $\Gamma = 10$ nm and $D = 5$ nm for cobalt. These geometrical parameters give the biggest drop in the critical current density in our calculations. From this figure, we observe that for the first normal mode the current density changes by 14%, and this variation decreases when we increase the normal mode number.

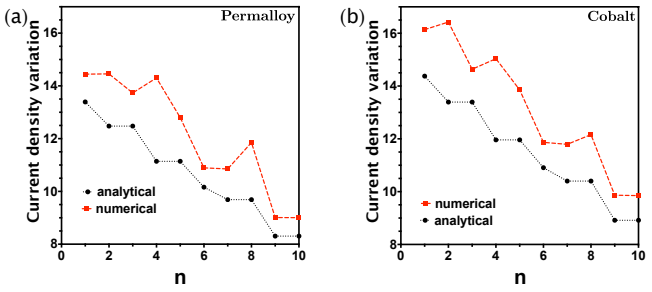

FIG. 10. Critical current density variation (percentage) from Eqns. (22) and (23) as a function of the normal modes. (a) The free and fixed layers are made of permalloy with $\Gamma = 20$ nm and $D = 5$ nm. (b) The free layer is made of permalloy and the fixed layer is made of cobalt with $\Gamma = 10$ nm and $D = 5$ nm. The dot black line corresponds to $\Delta J^N_{C,n}(\Gamma, D)$. The dashed red line corresponds to $\Delta J^A_{C,mj}(\Gamma, D)$.

The steps evidenced in Figs. 7 and 10, related to the analytical results, occur because there is a degeneracy

of the normal modes in this approximation. The non-monotonic behavior of Fig. 10, comes mainly from the fact that the magnetostatic interaction field does not couple equivalently with each normal mode. In this way, this field significantly affects certain normal modes.

In this work we have analysed the "parallel-state", where the magnetization of both the free and the fixed layer are pointing in the same direction and sense. In this configuration, the magnetostatic interaction field between the ferromagnetic layers is pointing opposite to the applied field, for this reason both the frequencies and the critical current decrease when the interaction field increases. On the other hand, if the system is in the "anti-parallel state", i.e, the magnetization of the free and the fixed layer are pointing in the same direction and different sense, the magnetostatic interaction field is pointing in the same sense that the applied field. Therefore, Eq. (13) changes its sign from minus to plus, and then the frequencies and the critical current increase when the magnetostatic interaction field increases. The above can be understood directly from Eqns. (14) and (20).

IV. CONCLUSIONS

As a summary, by means of numerical calculations and an analytical model, we have studied the modification of the free layer spin wave modes of a nano-pillar oscillator due to the magnetostatic interaction between the free and the fixed layer. For these modes we have studied both their frequencies and shapes as a function of the fixed layer thickness, non-magnetic spacer thickness and the magnetic material of the fixed layer. It has been found that the frequencies as well as the critical current density of the lower modes decreases when the fixed layer becomes thicker or the non-magnetic spacer becomes thinner, effects that may be significant. We also observe that the shape of the lower normal modes do not change in spite of the fixed layer thickness changes. At higher normal modes, the fixed layer does not affect the frequencies and the critical current densities since in this case the exchange interaction is more relevant than the magnetostatic interaction between the layers. These results can be used to modify the natural frequencies of oscillation or the critical current densities necessary to induce the magnetization self-oscillations without altering the shape of the lower modes for the free layer, which from an experimental or practical point of view may be useful for the study of the excitation of the spin waves and also for the design of systems with lower power consumption.

ACKNOWLEDGEMENTS

We acknowledge financial support in Chile from FONDECYT 1161018, 1160198, 1170781 and 11160985, Financiamiento Basal para Centros Científicos y Tecnológicos de Excelencia FB 0807, and AFOSR Neuromorphics Inspired Science FA9550-16-1-0384. S.O. acknowledge to PAI-CONICYT Grant No. 79140036.

Appendix A: Expressions for the free energy as a function of a and a^*

The normalized free energy is given by

$$\mathcal{U} = \frac{1}{4\pi M_s^2}\int(\mathcal{W}_Z + \mathcal{W}_E + \mathcal{W}_D + \mathcal{W}_I)dV \ , \qquad \text{(A1)}$$

where $\mathcal{W}_Z$, $\mathcal{W}_E$, $\mathcal{W}_D$ and $\mathcal{W}_I$ represent the Zeeman, exchange, self-magnetostatic and the inter layers magnetostatic interaction energy densities, respectively. The integration is over the free layer volume.

1. External field energy

A constant field is applied in the x direction, then the associated Zeeman energy density is given by

$$\mathcal{W}_Z = -\vec{H}\cdot\vec{M} = -H_x M_x = -H_x M_s(1 - aa^*) \ . \quad \text{(A2)}$$

The constant term does not affect the dynamics, so the Zeeman energy associated with the applied magnetic field is an expression of second order:

$$\mathcal{U}_Z = h_x \int aa^* dV \ , \qquad \text{(A3)}$$

with $h_x = H_x/(4\pi M_s)$ the normalised applied field.

2. Exchange energy

The exchange energy density in cartesian coordinates is given by

$$\mathcal{W}_E = A\left[(\vec{\nabla}m_x)^2 + (\vec{\nabla}m_y)^2 + (\vec{\nabla}m_z)^2\right] \ , \qquad \text{(A4)}$$

where A is the exchange constant. Thus, the energy expanded until fourth order is

$$\mathcal{U}_E \approx h_E \int \left[\vec{\nabla}a\cdot\vec{\nabla}a^* + \frac{1}{4}a^2(\vec{\nabla}a^*)^2 + \frac{1}{4}a^{*2}(\vec{\nabla}a)^2\right] R^2 dV \ , \qquad \text{(A5)}$$

with $h_E = A/(2\pi M_s^2 R^2) = (l_E/R)^2$, with l_E the exchange length.

3. Demagnetizing free layer energy

The self-magnetostatic energy density is given by

$$\mathcal{W}_D = -\frac{1}{2}\vec{H}_D\cdot\vec{M} \ . \qquad \text{(A6)}$$

For the purpose of determining the demagnetizing field of the thin disk, the free layer magnetization is assumed uniform in its thickness and then does not depend on the z coordinate. First, we calculate the magnetostatic potential Φ and then the demagnetizing field through the relation $\vec{H}_D = -\vec{\nabla}\Phi$. The magnetostatic potential is given by

$$\Phi(\vec{x}) = \int \frac{\sigma_M}{|\vec{x}-\vec{x}'|} dS' + \int \frac{\rho_M}{|\vec{x}-\vec{x}'|} dV' \ , \tag{A7}$$

where $\sigma_M = \hat{n}\cdot\vec{M}(\vec{x}')$ is the effective surface magnetic charge density on the surface of the disk (top, bottom and side), and $\rho_M = -\vec{\nabla}\cdot\vec{M}(\vec{x}')$ is the effective volumetric magnetic charge density. The Green's function can be written in cylindrical coordinates as:

$$\frac{1}{|\vec{x}-\vec{x}'|} = \sum_{m=-\infty}^{\infty} e^{im(\phi-\phi')} \int_0^\infty J_m(k\rho)J_m(k\rho')e^{-k|z-z'|}dk \ . \tag{A8}$$

In order to calculate the demagnetizing field averaged over the thickness of the disk ($\langle\vec{H}_D\rangle_z = \frac{1}{L}\int_0^L \vec{H}_D dz$), we separate the calculation in two parts.

a. Surface magnetic charges at the top and bottom

The surface magnetic charges at the top and bottom of the free layer disk give rise to a magnetic field along the z direction, which normalised is given by

$$\begin{aligned}\langle h_D^z\rangle_z =& -m_z + \frac{2}{4\pi L}\sum_{m=-\infty}^{\infty}\int_0^\infty f(kL)J_m(k\rho)e^{im\phi} \\ &\times\left[\int dS' J_m(k\rho')m_z(\rho',\phi')e^{-im\phi'}\right]dk \ ,\end{aligned} \tag{A9}$$

with $f(u)\equiv\exp(-u)-1+u$, and the sub-index indicates average over z.

b. Volumetric and surface magnetic charges at the edge

The surface magnetic charges at the edge of the free layer disk plus the volumetric magnetic charges give rise to a magnetic field in the plane of the free layer, which normalised is given by

$$\begin{aligned}\langle\vec{h}_D^{||}\rangle_z =& -\frac{1}{2\pi L}\sum_{m=-\infty}^{\infty}\int_0^\infty \frac{f(kL)}{k^2}\vec{\nabla}(J_m(k\rho)e^{im\phi}) \\ &\times\left[\int dS'\vec{\nabla}(J_m(k\rho')e^{-im\phi'})\cdot\vec{m}_{||}(\rho',\phi')\right]dk \ ,\end{aligned} \tag{A10}$$

where $\vec{m}_{||} = m_x\hat{x} + m_y\hat{y}$, and the sub-index indicates average over z.

Thus, the demagnetizing energy is given by

$$\mathcal{U}_D = -\frac{1}{2}\int\left(\langle h_D^z\rangle_z + \langle\vec{h}_D^{||}\rangle_z\right)\cdot\vec{m}\,dV \ . \tag{A11}$$

4. Magnetostatic interaction energy between the layers

The energy density associated with the interaction of the free layer with the fixed layer magnetostatic field is given by

$$\mathcal{W}_I = -\vec{H}_I\cdot\vec{M} \ . \tag{A12}$$

In order to calculate the magnetostatic field, the same procedure as in section A 3 is used, that is, we first determine the magnetostatic potential produced by the fixed layer considering that it is uniformly magnetized, with $\vec{M}_{\rm fix} = M_{\rm fix}\hat{x}$. Therefore this magnetostatic potential is given by

$$\Phi(\vec{x}) = \int\frac{\hat{n}\cdot\vec{M}_{\rm fix}(\vec{x}')}{|\vec{x}-\vec{x}'|}dS' \ , \tag{A13}$$

with $\hat{n}\cdot\vec{M}_{\rm fix} = M_{\rm fix}\cos\phi'$ we obtain

$$\Phi(\vec{x}) = 2\pi M_{\rm fix}R\cos(\phi)\int_0^\infty \frac{J_1(q)J_1\left(\frac{q\rho}{R}\right)(e^{\frac{q\Gamma}{R}}-1)e^{-\frac{qz}{R}}}{q}dq \ . \tag{A14}$$

If we define the following dimensionless quantities $l = L/R$, $h = \Gamma/R$, $d = D/R$, and then averaging the normalized magnetostatic field over the free layer thickness, i.e. $\langle\vec{h}\rangle_z = -\frac{1}{4\pi M_s L}\int_{\Gamma+D}^{\Gamma+D+L}\vec{\nabla}\Phi\,dz$, we get

$$\begin{aligned}\langle h_I^x\rangle_z =& -\frac{R}{4L}\frac{M_{\rm fix}}{M_s}\int_0^\infty f(h,l,d,q)J_1(q) \\ &\times\left[J_0\left(\frac{q\rho}{R}\right) - J_2\left(\frac{q\rho}{R}\right)\cos(2\phi)\right]dq \ ,\end{aligned} \tag{A15a}$$

$$\langle h_I^y\rangle_z = \frac{R}{4L}\frac{M_{\rm fix}}{M_s}\int_0^\infty f(h,l,d,q)J_1(q)J_2\left(\frac{q\rho}{R}\right)\sin(2\phi)\,dq \ , \tag{A15b}$$

$$\langle h_I^z\rangle_z = \frac{R}{2L}\frac{M_{\rm fix}}{M_s}\int_0^\infty f(h,l,d,q)J_1(q)J_1\left(\frac{q\rho}{R}\right)\cos(\phi)\,dq, \tag{A15c}$$

with $f(h,l,d,q) = (1-e^{-qh})(1-e^{-ql})e^{-qd}/q$. Finally the energy associated with the interaction between the ferromagnetic layers is given by

$$\mathcal{U}_I = -\int\langle\vec{h}_I\rangle_z\cdot\vec{m}\,dV \ . \tag{A16}$$

Appendix B: Expressions for the free energy as a function of the a_{mj} and a^*_{mj}

In this section we show the dependence of the energies as a function of the a_{mj} and a^*_{mj} variables.

1. External field energy

The external field energy is simply:

$$\mathcal{U}_Z = h_x\sum_{mj}a_{mj}a^*_{mj} \ . \tag{B1}$$

2. Exchange energy

The exchange energy is composed of two terms, one of second and the other of fourth order, i.e. $\mathcal{U}_E = \mathcal{U}_E^{(2)} + \mathcal{U}_E^{(4)}$:

$$\mathcal{U}_E^{(2)} = h_E \sum_{mj} \chi_{mj}^2 a_{mj} a_{mj}^* \ , \tag{B2a}$$

$$\mathcal{U}_E^{(4)} = -\frac{h_E}{2} \sum_{\substack{m_1 j_1 \\ m_2 j_2}} \sum_{\substack{m_3 j_3 \\ m_4 j_4}} (a_{m_1 j_1} a_{m_2 j_2} a_{m_3 j_3}^* a_{m_4 j_4}^* + c.c) \times \delta_{m_3+m_4}^{m_1+m_2} i^E_{m_1 j_1 m_2 j_2 m_3 j_3 m_4 j_4} \ , \tag{B2b}$$

where

$$i^E_{m_1 j_1 m_2 j_2 m_3 j_3 m_4 j_4} \equiv \chi_{m_1 j_1} \chi_{m_2 j_2} N_{m_1 j_1} N_{m_2 j_2} N_{m_3 j_3} N_{m_4 j_4} \times \int_0^1 J_{m_1+1}(\chi_{m_1 j_1} x) J_{m_2-1}(\chi_{m_2 j_2} x) \times J_{m_3}(\chi_{m_3 j_3} x) J_{m_4}(\chi_{m_4 j_4} x) x dx \ . \tag{B3}$$

3. Free layer demagnetizing energy

The free layer demagnetizing energy associated with magnetization on the x-axis and y-axis will be composed of four terms of orders one, two, three and four respectively, i.e. $\mathcal{U}_D^{xy} = \mathcal{U}_D^{xy(1)} + \mathcal{U}_D^{xy(2)} + \mathcal{U}_D^{xy(3)} + \mathcal{U}_D^{xy(4)}$, whose expressions are:

$$\mathcal{U}_D^{xy(1)} = \frac{1}{2\sqrt{2}} \sum_j [(a_{-2j} - a_{2j}^*) + c.c] I^2(l)_{(0,0,j)} \ , \tag{B4a}$$

$$\begin{aligned}
\mathcal{U}_D^{xy(2)} = & \sum_{\substack{m_1 j_1 \\ m_2 j_2}} \{ a_{m_1 j_1} a_{m_2 j_2}^* \sum_j \\
& \times [(\delta_{-2}^{m_1-m_2} + \delta_2^{m_1-m_2}) i^3_{2j m_1 j_1 m_2 j_2} I^2(l)_{(0,0,j)} \\
& - 2\delta_0^{m_1-m_2} i^3_{0 j m_1 j_1 m_2 j_2} I^1(l)_{(0,0,j)}] \\
& - \frac{1}{8}(-1)^{m_1} (a_{m_1 j_1} - (-1)^{m_1} a^*_{-m_1 j_1}) \\
& \times (a_{m_2 j_2} - (-1)^{m_2} a^*_{-m_2 j_2}) (\delta_{-2}^{m_1+m_2} I^2(l)_{(m_1,j_1,j_2)} \\
& + \delta_2^{m_1+m_2} I^3(l)_{(m_1,j_1,j_2)} + 2\delta_0^{m_1+m_2} I^1(l)_{(m_1,j_1,j_2)}) \} \ ,
\end{aligned} \tag{B4b}$$

$$\begin{aligned}
\mathcal{U}_D^{xy(3)} = & -\frac{1}{4\sqrt{2}} \sum_{\substack{m_1 j_1 \\ m_2 j_2 \\ m_3 j_3}} \{ (a_{m_1 j_1} - (-1)^{m_1} a^*_{-m_1 j_1}) \\
& \times a_{m_2 j_2} a^*_{m_3 j_3} (\delta_{-2}^{m_1+m_2-m_3} - \delta_2^{m_1+m_2-m_3}) \\
& \sum_j [i^4_{2j m_1 j_1 m_2 j_2 m_3 j_3} I^2(l)_{(0,0,j)}] \\
& - \frac{1}{\sqrt{2}} (-1)^{m_3} (a_{m_3 j_3} - (-1)^{m_3} a^*_{-m_3 j_3}) a_{m_1 j_1} a^*_{m_2 j_2} \\
& \times (\delta_{-2}^{m_1-m_2+m_3} \sum_j [i^3_{-m_3-2j m_1 j_1 m_2 j_2} I^2(l)_{(m_3,j_3,j)}] \\
& - \delta_2^{m_1-m_2+m_3} \sum_j [i^3_{-m_3+2j m_1 j_1 m_2 j_2} I^3(l)_{(m_3,j_3,j)}]) \} \ ,
\end{aligned} \tag{B4c}$$

$$\begin{aligned}
\mathcal{U}_D^{xy(4)} = & \frac{1}{8} \sum_{\substack{m_1 j_1 \\ m_2 j_2}} \sum_{\substack{m_3 j_3 \\ m_4 j_4}} \{ (a_{m_4 j_4} - (-1)^{m_4} a^*_{-m_4 j_4}) \\
& \times (a_{m_1 j_1} - (-1)^{m_1} a^*_{-m_1 j_1}) a_{m_2 j_2} a^*_{m_3 j_3} \\
& (\delta_{-2}^{m_1+m_2-m_3+m_4} \sum_j [i^4_{m_4+2j m_1 j_1 m_2 j_2 m_3 j_3} I^2(l)_{(m_4,j_4,j)}] \\
& + \delta_2^{m_1+m_2-m_3+m_4} \sum_j [i^4_{m_4-2j m_1 j_1 m_2 j_2 m_3 j_3} I^3(l)_{(m_4,j_4,j)}] \\
& + 2\delta_0^{m_1+m_2-m_3+m_4} \sum_j [i^4_{m_4 j m_1 j_1 m_2 j_2 m_3 j_3} I^1(l)_{(m_4,j_4,j)}]) \\
& - a_{m_1 j_1} a^*_{m_2 j_2} a_{m_3 j_3} a^*_{m_4 j_4} \sum_{j' j''} [i^3_{m_1-m_2 j' m_1 j_1 m_2 j_2} \\
& \times (\delta_{m_4-2}^{m_1-m_2+m_3} i^3_{m_1-m_2+2j'' m_3 j_3 m_4 j_4} I^2(l)_{(m_1-m_2,j',j'')} \\
& + \delta_{m_4+2}^{m_1-m_2+m_3} i^3_{m_1-m_2-2j'' m_3 j_3 m_4 j_4} I^3(l)_{(m_1-m_2,j',j'')} \\
& - 2\delta_{m_4}^{m_1-m_2+m_3} i^3_{m_1-m_2 j'' m_3 j_3 m_4 j_4} I^1(l)_{(m_1-m_2,j',j'')})] \} \ .
\end{aligned} \tag{B4d}$$

The energy associated with the z component of the magnetization is composed of a term of order two and another of order four, i.e. $\mathcal{U}_D^z = \mathcal{U}_D^{z\,(2)} + \mathcal{U}_D^{z\,(4)}$:

$$\mathcal{U}_D^{z\,(2)} = \frac{1}{4} \sum_{m_1 j_1 j_2} (\delta_{j_2}^{j_1} - 2I^1(l)_{(m_1,j_1,j_2)}) \times (a_{m_1 j_1} + (-1)^{m_1} a^*_{-m_1 j_1})((-1)^{m_1} a_{-m_1 j_2} + a^*_{m_1 j_2}) \ , \tag{B5a}$$

$$\begin{aligned}
\mathcal{U}_D^{z\,(4)} = & -\frac{1}{4} \sum_{\substack{m_1 j_1 \\ m_2 j_2}} \sum_{\substack{m_3 j_3 \\ m_4 j_4}} \delta_{-m_4}^{m_1+m_2-m_3} a_{m_2 j_2} a^*_{m_3 j_3} \\
& \times (a_{m_4 j_4} + (-1)^{m_4} a^*_{-m_4 j_4}) (a_{m_1 j_1} + (-1)^{m_1} a^*_{-m_1 j_1}) \\
& \times (i^4_{m_4 j_4 m_1 j_1 m_2 j_2 m_3 j_3} - \sum_{j_5} 2 i^4_{m_4 j_5 m_1 j_1 m_2 j_2 m_3 j_3} I^1(l)_{(m_4,j_4,j_5)}) \ .
\end{aligned} \tag{B5b}$$

with

$$I^1(l)_{(l_1,j_1,j_2)} = N_{l_1 j_1} N_{l_1 j_2} J_{l_1}(\chi_{l_1 j_1}) J_{l_1}(\chi_{l_1 j_2}) \times \int_0^\infty dq \frac{f(ql) q^2 J'_{l_1}(q)^2}{l(q^2 - (\chi_{l_1 j_1})^2)(q^2 - (\chi_{l_1 j_2})^2)} \ , \tag{B6a}$$

$$I^2(l)_{(l_1,j_1,j_2)} = N_{l_1 j_1} N_{l_1+2 j_2} J_{l_1}(\chi_{l_1 j_1}) J_{l_1+2}(\chi_{l_1+2 j_2}) \times \int_0^\infty dq \frac{f(ql) q^2 J'_{l_1}(q) J'_{l_1+2}(q)}{l(q^2 - (\chi_{l_1 j_1})^2)(q^2 - (\chi_{l_1+2 j_2})^2)} \ , \tag{B6b}$$

$$I^3(l)_{(l_1,j_1,j_2)} = N_{l_1 j_1} N_{(l_1-2) j_2} J_{l_1}(\chi_{l_1 j_1}) J_{l_1-2}(\chi_{l_1-2 j_2})$$

$$\times \int_0^\infty dq \frac{f(ql)q^2 J'_{l_1}(q)J'_{l_1-2}(q)}{l(q^2-(\chi_{l_1 j_1})^2)(q^2-(\chi_{l_1-2 j_2})^2)} \ . \quad \text{(B6c)}$$

with $f(ql) \equiv e^{-ql} + ql - 1$ and

$$i^3_{ljm_1j_1m_2j_2} = N_{lj}N_{m_1j_1}N_{m_2j_2} \times \int_0^1 J_l(\chi_{lj}x)J_{m_1}(\chi_{m_1j_1}x)J_{m_2}(\chi_{m_2j_2}x)xdx \ , \quad \text{(B7)}$$

$$i^4_{ljm_1j_1m_2j_2m_3j_3} = N_{lj}N_{m_1j_1}N_{m_2j_2}N_{m_3j_3} \times \int_0^1 J_l(\chi_{lj}x)J_{m_1}(\chi_{m_1j_1}x)J_{m_2}(\chi_{m_2j_2}x)J_{m_3}(\chi_{m_3j_3}x)xdx \ . \quad \text{(B8)}$$

4. Magnetostatic interaction energy between the layers

The magnetostatic interaction energy between the layers associated with the x component of the free layer magnetization is composed of a term of order two:

$$\mathcal{U}_I^{x(2)} = \frac{1}{2l}\sum_{\substack{m_1j_1\\m_2j_2}} [2a_{m_1j_1}a^*_{m_2j_2}i^3_{0jm_1j_1m_2j_2}\delta^{m_1}_{m_2}I_{0j}(h,l,d) - (a_{m_1j_1}a^*_{m_2j_2}+c.c)i^3_{2jm_1j_1m_2j_2}\delta^2_{m_1-m_2}I_{2j}(h,l,d)] \ . \quad \text{(B9)}$$

The analogous interaction energy associated with the y component of the free layer magnetizaton is composed of a term of order one and another of order three, i.e. $\mathcal{U}_I^y = \mathcal{U}_I^{y(1)} + \mathcal{U}_I^{y(3)}$:

$$\mathcal{U}_I^{y(1)} = \frac{1}{4\sqrt{2}l}\sum_j (a^*_{2j} - a_{-2j} + a_{2j} - a^*_{-2j})I_{2j}(h,l,d) \ , \quad \text{(B10a)}$$

$$\mathcal{U}_I^{y(3)} = -\frac{1}{8\sqrt{2}l}\sum_{\substack{m_1j_1\\m_2j_2\\m_3j_3}} \delta^2_{m_1+m_2-m_3} i^4_{2jm_1j_1m_2j_2m_3j_3} \times [(a^*_{m_1j_1} - (-1)^{m_1}a_{-m_1j_1})a^*_{m_2j_2}a_{m_3j_3} + c.c]I_{2j}(h,l,d) \ . \quad \text{(B10b)}$$

The interaction energy associated with z component magnetization is composed of a term of order one and another of order three, i.e. $\mathcal{U}_I^z = \mathcal{U}_I^{z(1)} + \mathcal{U}_I^{z(3)}$:

$$\mathcal{U}_I^{z(1)} = \frac{1}{2\sqrt{2}l}\sum_j (a_{1j} - a^*_{-1j} + a^*_{1j} - a_{-1j})I_{1j}(h,l,d) \ , \quad \text{(B11a)}$$

$$\mathcal{U}_I^{z(3)} = -\frac{1}{4\sqrt{2}l}\sum_{\substack{m_1j_1\\m_2j_2\\m_3j_3}} \delta^1_{m_1+m_2-m_3} i^4_{1jm_1j_1m_2j_2m_3j_3} \times [(a_{m_1j_1} + (-1)^{m_1}a^*_{-m_1j_1})a_{m_2j_2}a^*_{m_3j_3} + c.c]I_{1j}(h,l,d) \ , \quad \text{(B11b)}$$

with

$$I_{nj}(h,l,d) = N_{nj}J_n(\chi_{nj})\int_0^\infty dqJ_1(q)J'_n(q)\frac{g(q,h,l,d)}{(q^2-\chi^2_{nj})} \ , \quad \text{(B12a)}$$

$$g(q,h,l,d) = (1-e^{-qh})(1-e^{-ql})e^{-qd} \ . \quad \text{(B12b)}$$

Appendix C: Effect of the external field

In addition to results showed in the main text, in this section we address the effect of the external field on the normal modes and the critical current. For these calculations we use a fixed layer of CoFe, which has a saturated magnetization of $M_{\rm fix} = 1800$ emu/cm^3 (see Ref. 37). Fig. 11 illustrates the first three frequencies of the normal modes as a function of the fixed layer thickness for different normalized external applied fields. From the figure we observe that the frequencies increase when we increase the normalized external field. In Fig. 11(a), the normalized applied field is $h_x = 0.1$ while in Fig. 11(b) the normalized applied field is $h_x = 0.25$. In the first case, we cannot consider a fixed layer thickness bigger than 8 nm, since the magnetostatic field of the fixed layer, that is opposite to the external applied field, could revert the magnetization of the free layer. If we increase the normalized applied field to $h_x = 0.25$, the magnetization of the free layer is more stable than the previous case. Therefore, it is possible to increase the magnetostatic field due to the fixed layer by increasing the thickness of the fixed layer.

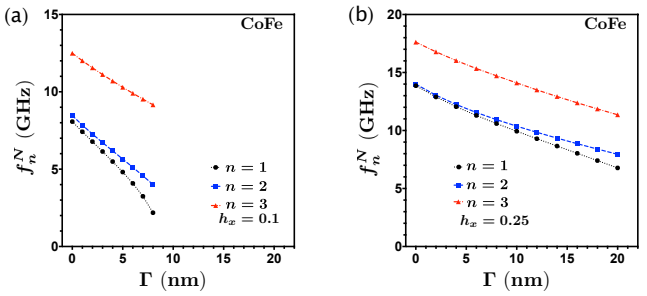

FIG. 11. Frequencies of the first three normal modes as a function of the fixed layer thickness. The free layer is made of permalloy and the fixed layer is made of CoFe. The thickness of the Cu spacer is $D = 5$ nm. (a) The applied field is $h_x = 0.1$. (b) The applied field is $h_x = 0.25$.

We also study the dependency of the frequencies of the first three normal modes on the non-magnetic spacer thickness. In Fig. 12 we observe that the frequencies decrease when the non-magnetic spacer thickness diminishes. In Fig. 12(a) the normalized applied field is $h_x = 0.1$ and the the thickness of the fixed layer is $\Gamma = 8$ nm. In this case, the minimum value of D is 4 nm. In Fig. 12(b) the normalized applied field is $h_x = 0.25$ and

the thickness of the fixed layer is $\Gamma = 20$ nm. In this case the minimum value of D is 2 nm. Therefore, the magnetization of the free layer is more stable for $h_x = 0.25$ than for $h_x = 0.1$, even if we increase the fixed layer thickness from 8 nm to 20 nm.

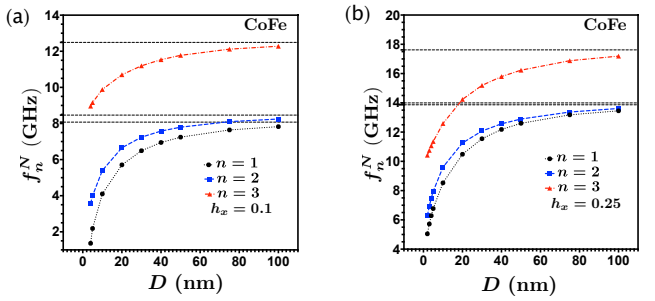

FIG. 12. Frequencies of the first three normal modes as a function of the non-magnetic spacer thickness. The free layer is made of permalloy and the fixed layer is made of CoFe. (a) The thickness of the fixed layer is $\Gamma = 8$ nm. (b) The thickness of the fixed layer is $\Gamma = 20$ nm. The horizontal dashed lines represent the frequencies of the normal modes without the effect of the fixed layer.

Finally, Fig. 13 illustrates the lowest critical current density for the first normal mode. We observe that the critical current increases when the normalized external applied field increases.

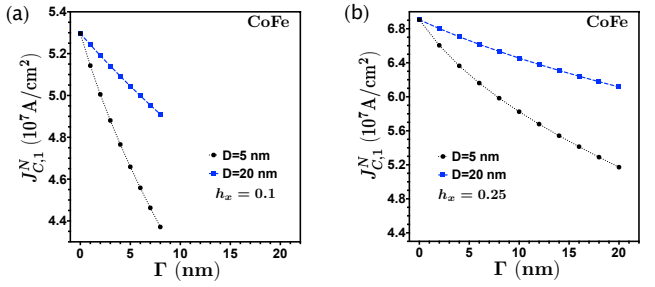

FIG. 13. Critical current density necessary to induce self-oscillations in the lowest normal mode as a function of the fixed layer thickness, at $D = 5$ nm (dots) and $D = 20$ nm (squares).

REFERENCES

[1] J. C. Slonczewski, Current-driven excitation of magnetic multilayers, J. Magn. Magn. Mater. 159 (1996) L1–L7. doi:10.1016/0304-8853(96)00062-5.

[2] L. Berger, Emission of spin waves by a magnetic multilayer traversed by a current, Phys. Rev. B 54 (13) (1996) 9353–9358. doi:10.1103/PhysRevB.54.9353.

[3] J. Z. Sun, Spin-current interaction with a monodomain magnetic body: A model study, Phys. Rev. B 62 (1) (2000) 570–578. doi:10.1103/PhysRevB.62.570.

[4] J. A. Katine, F. J. Albert, R. A. Buhrman, E. B. Myers, D. C. Ralph, Current-driven magnetization reversal and spin-wave excitations in Co/Cu/Co pillars, Phys. Rev. Lett. 84 (14) (2000) 3149–3152. doi:10.1103/PhysRevLett.84.3149.

[5] S. I. Kiselev, J. C. Sankey, I. N. Krivorotov, N. C. Emley, R. J. Schoelkopf, R. A. Buhrman, D. C. Ralph, Microwave oscillations of a nanomagnet driven by a spin-polarized current, Nature 425 (6956) (2003) 380–383. doi:10.1038/nature01967.

[6] M. Tsoi, A. G. M. Jansen, J. Bass, W.-C. Chiang, M. Seck, V. Tsoi, P. Wyder, Excitation of a Magnetic Multilayer by an Electric Current, Phys. Rev. Lett. 80 (19) (1998) 4281–4284. doi:10.1103/PhysRevLett.80.4281.

[7] A. Brataas, A. D. Kent, H. Ohno, Current-induced torques in magnetic materials, Nature Materials 11 (5) (2012) 372–381. doi:10.1038/nmat3311.

[8] K. L. Wang, J. G. Alzate, P. K. Amiri, Low-power non-volatile spintronic memory: STT-RAM and beyond, Journal of Physics D: Applied Physics 46 (7) (2013) 074003. doi:10.1088/0022-3727/46/7/074003.

[9] N. Locatelli, V. Cros, J. Grollier, Spin-torque building blocks, Nature Materials 13 (1) (2014) 11–20. doi:10.1038/nmat3823.

[10] J. Grollier, D. Querlioz, M. D. Stiles, Spintronic Nanodevices for Bioinspired Computing, Proceedings of the IEEE 104 (10) (2016) 2024–2039. doi:10.1109/JPROC.2016.2597152.

[11] D. C. Ralph, M. D. Stiles, Spin transfer torques, J. Magn. Magn. Mater. 320 (7) (2008) 1190–1216. doi:10.1016/j.jmmm.2007.12.019.

[12] S. Urazhdin, W. L. Lim, A. Higgins, Effect of polarizer dynamics on current-induced behaviors in magnetic nanopillars, Phys. Rev. B 80 (14) (2009) 144411. doi:10.1103/PhysRevB.80.144411.

[13] Z. Hou, Y. Liu, S. Cardoso, P. P. Freitas, H. Chen, C.-R. Chang, Dynamics of the reference layer driven by spin-transfer torque: Analytical versus simulation model, J. Appl. Phys 109 (11) (2011) 113914. doi:10.1063/1.3592973.

[14] M. Romera, E. Monteblanco, F. Garcia-Sanchez, B. Delaet, L. D. Buda-Prejbeanu, U. Ebels, Influence of interlayer coupling on the spin-torque-driven excitations in a spin-torque oscillator, Phys. Rev. B 95 (9) (2017) 094433. doi:10.1103/PhysRevB.95.094433.

[15] B. Dieny, V. S. Speriosu, S. S. P. Parkin, B. A. Gurney, D. R. Wilhoit, D. Mauri, Giant magnetoresistive in soft ferromagnetic multilayers, Phys. Rev. B 43 (1991) 1297(R). doi:10.1103/PhysRevB.43.1297.

[16] P. P. Freitas, R. Ferreira, S. Cardoso, F. Cardoso, Magnetoresistive sensors, J. Phys.: Condens. Matter 19 (2007) 165221. doi:10.1088/0953-8984/19/16/165221.

[17] U. Hartmann, Magnetic Multilayers and Giant Magnetoresistance: Fundamentals and Industrial Applications, Springer, 1986.

[18] R. Salikhov, R. Abrudan, F. Brssing, St. Buschhorn, M. Ewerlin, D. Mishra, F. Radu, I. A. Garifullin, H. Zabel, Precessional dynamics and damping in Co/Cu/Py spin valves, Appl. Phys. Lett. 99 (9) (2011) 092509. doi:10.1063/1.3633115.

[19] S. I. Kiselev, J. C. Sankey, I. N. Krivorotov, N. C. Emley, M. Rinkoski, C. Perez, R. A. Buhrman, D. C. Ralph, Current-Induced Nanomagnet Dynamics for Magnetic Fields Perpendicular to the Sample Plane, Phys. Rev. Lett. 93 (3) (2004) 036601. doi:10.1103/PhysRevLett.93.036601.

[20] J. Flipse, F. K. Dejene, B. J. van Wees, Comparison between thermal and current driven spin-transfer torque in nanopillar metallic spin valves, Phys. Rev. B 90 (10) (2014) 104411. doi:10.1103/PhysRevB.90.104411.

[21] O. J. Lee, V. S. Pribiag, P. M. Braganca, P. G. Gowtham, D. C. Ralph, R. A. Buhrman, Ultrafast switching of a nanomagnet by a combined out-of-plane and in-plane polarized spin current pulse, Appl. Phys. Lett. 95 (1) (2009) 012506. doi:10.1063/1.3176938.

[22] O. Ozatay, P. G. Gowtham, K. W. Tan, J. C. Read, K. A. Mkhoyan, M. G. Thomas, G. D. Fuchs, P. M. Braganca, E. M.

Ryan, K. V. Thadani, J. Silcox, D. C. Ralph, R. A. Buhrman, Sidewall oxide effects on spin-torque- and magnetic-field-induced reversal characteristics of thin-film nanomagnets, Nature Materials 7 (2008) 567. doi:10.1038/nmat2204.

[23] O. Boulle, V. Cros, J. Grollier, L. G. Pereira, C. Deranlot, F. Petroff, G. Faini, J. Barna, A. Fert, Shaped angular dependence of the spin-transfer torque and microwave generation without magnetic field, Nature Physics 3 (2007) 492. doi:10.1038/nphys618.

[24] N. Locatelli, A. Hamadeh, F.-A. Araujo, A. D. Belanovsky, P. N. Skirdkov, R. Lebrun, V. V. Naletov, K. A. Zvezdin, M. Muñoz, J. Grollier, O. Klein, V. Cros, G. de Loubens, Efficient Synchronization of Dipolarly Coupled Vortex-Based Spin Transfer Nano-Oscillators, Scientific Reports 5, 17039 (2015). doi:10.1038/srep17039.

[25] J. Bass, W. P. Pratt Jr, Spin-diffusion lengths in metals and alloys, and spin-flipping at metal/metal interfaces: an experimentalist's critical review, Journal of Physics: Condensed Matter 19 (18) (2007) 183201–41. doi:10.1088/0953-8984/19/18/183201.

[26] P. Bruno, C. Chappert, Oscillatory coupling between ferromagnetic layers separated by a nonmagnetic metal spacer, Phys. Rev. Lett. 67 (1991) 1602. doi:10.1103/PhysRevLett.67.1602.

[27] G. Finocchio, I. Krivorotov, M. Carpentieri, G. Consolo, B. Azzerboni, L. Torres, E. Martinez, L. Lopez-Diaz, Magnetization dynamics driven by the combined action of ac magnetic field and dc spin-polarized current, Journal of Applied Physics 99 (8) (2006) 08G507. doi:10.1063/1.2165136.

[28] P. Krivosik, C. E. Patton, Hamiltonian formulation of nonlinear spin-wave dynamics: Theory and applications, Phys. Rev. B 82 (18) (2010) 184428. doi:10.1103/PhysRevB.82.184428.

[29] G. M. Wysin, W. A. Moura-Melo, L. A. S. Mól, A. R. Pereira, Dynamics and hysteresis in square lattice artificial spin ice, New Journal of Physics 15 (2013) 045029. doi:10.1088/1367-2630/15/4/045029.

[30] R. Matsumoto, A. Chanthbouala, J. Grollier, V. Cros, A. Fert, K. Nishimura, Y. Nagamine, H. Maehara, K. Tsunekawa, A. Fukushima, S. Yuasa, Spin-Torque Diode Measurements of MgO-Based Magnetic Tunnel Junctions with Asymmetric Electrodes, Applied Physics Express 4 (6) (2011) 063001. doi:10.1143/APEX.4.063001.

[31] D. Mancilla-Almonacid, R. E. Arias, Instabilities of spin torque driven auto-oscillations of a ferromagnetic disk magnetized in plane, Phys. Rev. B 93 (22) (2016) 224416. doi:10.1103/PhysRevB.93.224416.

[32] G. Strang, Introduction to applied mathematics, Wellesley-Cambridge, 1986.

[33] S. I. Kiselev, J. C. Sankey, I. N. Krivorotov, N. C. Emley, A. G. F. Garcia, R. A. Buhrman, D. C. Ralph, Spin-transfer excitations of permalloy nanopillars for large applied currents, Phys. Rev. B 72 (6) (2005) 064430. doi:10.1103/PhysRevB.72.064430.

[34] R. Heindl, S. E. Russek, T. J. Silva, W. H. Rippard, J. A. Katine, M. J. Carey, Size dependence of intrinsic spin transfer switching current density in elliptical spin valves, Appl. Phys. Lett. 92 (26) (2008) 262504. doi:10.1063/1.2953980.

[35] E. Villamor, M. Isasa, L. E. Hueso, F. Casanova, Temperature dependence of spin polarization in ferromagnetic metals using lateral spin valves, Phys. Rev. B 88 (18) (2013) 184411. doi:10.1103/PhysRevB.88.184411.

[36] B. H. M. Bauer, J. Fassbender, R. L. Stamps, Switching behavior of a Stoner particle beyond the relaxation time limit, Phys. Rev. B 61 (5) (2000) 3410–3416. doi:10.1103/PhysRevB.61.3410.

[37] N. Banerjee, A. Aziz, M. Ali, J. W. A. Robinson, B. J. Hickey, M. G. Blamire, Thickness dependence and the role of spin transfer torque in nonlinear giant magnetoresistance of permalloy dual spin valves, Phys. Rev. B 82 (22) (2010) 224402. doi:10.1103/PhysRevB.82.224402.